RSC Advances

ROYAL SOCIETY OF CHEMISTRY

www.rsc.org/advances

Cubic and Tetragonal Ferrite Crystal Structures for Copper Ion Immobilization in Iron-rich Ceramic Matrix

Yuanyuan Tang[a,*], Kaimin Shih[b], Chengshuai Liu[c], Changzhong Liao[b]

[a] School of Environmental Science and Engineering, South University of Science and Technology of China, 1088 Xueyuan Blvd, Nanshan District, Shenzhen 518055, P. R. China

[b] Department of Civil Engineering, The University of Hong Kong, Pokfulam Road, Hong Kong SAR, P. R. China

[c] State Key Laboratory of Environmental Geochemistry, Institute of Geochemistry, Chinese Academy of Sciences, Guiyang 550009, P. R. China

[*] Corresponding author: Tel: +86-88015460; E-mail address: tangyy@sustc.edu.cn

Abstract

This study proposed a strategy by reusing the incineration ash of municipal wastewater sludge as ceramic materials to immobilize copper. After sintering the mixture of CuO and sludge ash, hematite (α-Fe_2O_3, one major component) incorporated copper into

cubic $CuFe_2O_4$. To observe copper incorporation mechanisms, mixtures of $CuO+\alpha-Fe_2O_3$ were sintered from 650 to 1050 ^oC, and different copper incorporation behavior was detected. A low temperature $CuFe_2O_4$ phase with tetragonal structure was detected at 750 ^oC, and the cubic $CuFe_2O_4$ developed at 1000 ^oC. The incorporation efficiencies were first quantitatively determined by Rietveld refinement analysis of the X-ray diffraction data. The maximum copper incorporation into tetragonal and cubic $CuFe_2O_4$ reached around 80% and 73%, respectively. The leachability analysis pointed to superiority of both copper ferrites in stabilizing copper, suggesting a promising technique for incorporating copper into the iron-rich ceramic matrix. Both tetragonal and cubic $CuFe_2O_4$ were observed with incongruent leaching behavior, but the lower copper concentrations and higher [Cu]/[Fe] ratio in tetragonal $CuFe_2O_4$ leachates indicates its higher capacity for copper stabilization. With high transformation ratio into $CuFe_2O_4$ phases and dramatic reduction in metal leachability, the beneficial use of sludge ash to immobilize hazardous metal contaminated soil may be potentially succeeded.

Keywords

Municipal wastewater sludge; Copper ferrite; Quantification; Ceramics; Leaching; Immobilization

1. Introduction

The release of metals from mine activities to the surrounded sites can pose severe soil contamination, and may last for a long time without remediation.[1,2] Once in the soil, the metal pollutants may disperse mechanically and undergo weathering reactions, leading to metal ion distribution within the soil system in forms more mobile than the original ones.[3] Remediation approaches such as soil flushing, vacuum extraction, electro reclamation, bioremediation, and soil washing[4] are employed for metal-contaminated soil, but methods above are highly challenging and expensive for a large scale remediation.[5,6] Other investigators have also attempted to immobilize hazardous metals in contaminated soil by adding amendments that are able to adsorb, complex, or (co)precipitate elements in the soil.[7-9] The suggested copper immobilization mechanisms were reported to precipitate as copper carbonates and oxy-hydroxides, and formation of SO_4^{2-} or PO_4^{3-} complexes.[8] However, the mobility of heavy metals such as copper in soil is strongly pH dependent, and usually reaches the lowest value at slightly alkaline.[8] Once in acidic conditions, the immobilization effect of copper will be destroyed.[8,10]

By adding aluminum-rich materials into hazardous metal waste, the metals can be stabilized through well-controlled thermal treatment schemes.[11-14] By thermally reacting with alumina and kaolinite precursors, the nickel and copper in the spinel-type crystalline structure were found to have substantial reduction in their

leachability under acidic environments.

Sewage sludge (municipal wastewater sludge) is generated with huge quantity in urban environments, resulting from the accumulation of solids through wastewater treatment.[15] With complex and variable organic and inorganic substances, sewage sludge may contain viable pathogens and parasites as well as a variety of potentially toxic elements and compounds.[16] The amount of sludge produced annually is keeping dramatic increase all over the world.[17] In Europe, the production of dry sewage sludge is in average 90 g per person per day,[18,19] and there will be an increase of 50% by year.[18] While in Hong Kong, the amount of sludge will increase from the current quantity of about 800 tons per day to some 1,500 tons per day by 2014, and subsequently over 2,000 tons per day in 2020.[20] The disposal of sewage sludge is one of the most difficult problems to be solved, and the need to achieve a sustainable sludge management strategy has become of global concern.[21] Incineration has become an alternative to largely reduce the sludge volume, destruct pathogen agents, and remove organic pollutants for easier and safer handling and disposal.[17] Sludge incineration technology, as one of the most attractive disposal methods in the world,[18,22] was also chosen by Hong Kong government as the core treatment technology to resolve sludge problems.[20] Nevertheless, approximately 30% of the solids remain as residues after sludge incineration.[23] With further development of the incineration technology, the subsequent disposal of incineration residues is becoming a serious concern.[24,25]

Since sewage sludge ash always contains aluminum, silicon, and iron as the main components,[26,27] as a waste-to-resource technology, the use of sludge resulting from wastewater treatment processes has attracted much attention.[28] More than 70% of the total amount of sewage sludge generated in Hong Kong is through the chemically enhanced primary treatment (CEPT).[29] CEPT involves the use of chemical coagulants (such as alum, lime, ferric chloride, and polyaluminum chloride) to induce coagulation or flocculation of the suspended particles.[28,30] Once the incineration technology was adopted, iron and/or aluminum might become the main components in the ash after sludge incineration process. Therefore, it is predicted that the sludge ash may be potentially used to stabilize metals in contaminated soils. In this study, the sewage sludge ash will be reused and its potential for effectively stabilizing hazardous copper during the sintering process will be evaluated. Furthermore, to quantify the reaction mechanisms and immobilization efficiencies, the simulated system will also be analyzed to assist in the exploration of metal incorporation processes. A prolonged leaching experiment will be carried out to examine the copper stabilization effect, and the leaching behavior of the sintered products will be further discussed.

2. Experimental

The collected CEPT sludge sample was first dried at 105 ^{o}C, and the weight loss of the sludge calcined at a temperature range of 200-1000 ^{o}C was illustrated in Figure S1.

111 The weight of the dried sludge significantly reduced from 200 to 500 ^{o}C, and kept
112 stable afterwards. The ash from 900 ^{o}C and 30 min fired sludge was ground into
113 powder for elemental composition analysis by X-ray fluorescence spectroscopy (XRF)
114 (JEOL JSX-3201Z). Normalization into metal oxides (Figure S2) shows Si, Fe, Ca
115 and Al to be the major constituents in the ash. The XRD pattern (Figure S3) further
116 indicates predominant iron-containing crystalline phase as hematite (Fe_2O_3), while Si,
117 Ca and Al are mainly contained in hauyne ($Na_6Ca_2Al_6Si_6O_{24}(SO_4)_2$), anhydrite
118 ($CaSO_4$), and a type of zeolite ($Na_6(AlSiO_4)_6$). Works by others[31] also reported the
119 existence of aluminosilicate and anhydrite phases in the sewage sludge ash.
120
121 The 900 ^{o}C and 30 min fired sludge was used as soil amendment, and mixed with
122 copper oxide (Sigma Aldrich) which was simulated as the predominant pollutant of
123 the contaminated mining areas. Since both aluminum and iron will potentially react
124 with copper in the system, samples were first prepared by mixing CuO and the sludge
125 ash with the molar value of Al and Fe together as two times of Cu. The mixture was
126 then sintered at 950 ^{o}C, and the XRD pattern (Figure S4) shows Fe_2O_3 as the only
127 component reacting with copper and forming $CuFe_2O_4$ product phase. Therefore, the
128 CuO was further mixed with the sludge ash at a Cu:Fe molar ratio of 1:2 to guarantee
129 the maximum production of $CuFe_2O_4$ in the sludge ash system. To explore the
130 detailed mechanisms of copper incorporation, the Fe_2O_3 was used as iron-rich
131 material to react with CuO at a Cu:Fe molar ratio of 1:2. All mixing processes were
132 carried out by ball milling the powder in water slurry for 18 h. The slurry samples

were dried and homogenized by mortar grinding, pressed into 20-mm pellets at 480 MPa, and then fired. A sintering scheme with a 3-h dwelling time at the targeted temperature in a high-temperature furnace (LHT 02/16 LB, LBR, Nabertherm Inc.) was used for temperatures ranging from 650 to 1050 ^{o}C with furnace-controlled cooling.

Phase transformation during sintering was monitored using the powder X-ray diffraction (XRD) technique. The step-scanned XRD pattern of each powder sample was recorded by a Bruker D8 Advance X-ray powder diffractometer equipped with Cu Kα1,2 X-ray radiation source (40 kV 40 mA) and a LynxEye detector. The 2θ scanning range was 10 to 90º, and the step size was 0.02º with a scan speed of 0.8 s step^{-1}. Qualitative phase identification was executed by matching powder XRD patterns with those retrieved from the standard powder diffraction database of the International Centre for Diffraction Data (ICDD PDF-2, Release 2008). In hematite series, the crystalline phases in the products are all subjected to quantitative phase analysis using Topas 4-2, which employs the Rietveld refinement method.[32] The refinement quality was monitored by the reliability values provided in Table S1.

As one objective of this study was to distinguish the leaching characteristics of different copper-hosting phases, single-phase samples were considered preferable in the leaching experiment. The leaching experiments for CuO and copper-containing product phase(s) were conducted by a method modified from the U.S. Environmental

155 Protection Agency's SW-846 Method 1311: Toxicity Characteristic Leaching
156 Procedure (TCLP), with an acetic acid solution (extraction fluid #2, pH 2.9) used as the
157 leaching fluid. Each leaching vial was filled with 10 mL of leaching fluid and 0.5 g of
158 the powder sample and rotated end-over-end at 60 rpm for 0.75 to 22 days. At the end
159 of each agitation period, the leachates were filtered using 0.2-μm syringe filters, the pH
160 was determined, and the concentrations of all metals were derived by inductively
161 coupled plasma atomic emission (Perkin-Elmer Optima 3300 DV).
162
163 **3. Results and discussion**
164
165 *3.1. Potential of reusing municipal wastewater sludge ash for copper stabilization*
166
167 XRD patterns in Figure 1a demonstrate the phase transformation when the mixtures of
168 sludge ash and CuO were sintered at temperatures ranging from 650 to 1050 ^{o}C for 3
169 h. The peaks of $CuFe_2O_4$ spinel were detected after the 3-h sintering process at 750 ^{o}C,
170 even with very complicated compositions in the system. When the sintering
171 temperature increased to 850 ^{o}C, the $CuFe_2O_4$ spinel phase developed substantially
172 while peaks of CuO and Fe_2O_3 diminished accordingly. Further heating increased the
173 crystallinity and production of the $CuFe_2O_4$ spinel phase. Besides the formation of
174 $CuFe_2O_4$ spinel, other major components such as hauyne and zeolite kept
175 continuously growing, while anhydrite and quartz eventually decreased with elevated
176 temperatures. Although the decomposition temperature for anhydrite is usually higher

than 1000 °C,[33] the disappearance of anhydrite at temperature ≤ 850 °C in this experiment may be due to the conversion of calcium into the growing phases: hauyne and zeolite. Apart from phases discussed above, anorthite ($CaAl_2Si_2O_8$) — a main crystalline phase in glass-ceramics[34] kept relatively stable through out the sintering mechanism.

From the standard diffraction pattern of $CuFe_2O_4$ spinel (PDF#77-0010), the highest peak is at $2\theta \sim 35.5°$ but was overlapped by peaks of other phases. Therefore, the second highest peak at $2\theta \sim 62.7°$ was selected for further observation of the $CuFe_2O_4$ spinel in the sintered products (Figure 1b). The peak intensity of the $CuFe_2O_4$ spinel kept increasing after its first appearance at 750 °C, and a significant growth was observed when the sintering temperature increased from 750 to 850 °C. With further heating (≥ 950 °C), the spinel phase kept stable through out the sintering process. From the phase transformation during the sintering process of CuO + sewage sludge ash, iron was observed as the only component to incorporate copper, and the $CuFe_2O_4$ spinel was identified as the only copper-hosting product phase. It seems that other complicated compositions are not involved in the formation of $CuFe_2O_4$ spinel, and their existence might influence the efficiency of copper transformation. Therefore, the hematite (Fe_2O_3) without any other impurities was used as amendment to incorporate copper, and to further analyze the mechanisms of copper transformation in iron-rich systems.

199 *3.2. The mechanisms of copper incorporation in simulated iron-rich systems*

200

201 XRD patterns in Figure 2 illustrate the phase changes in CuO + Fe_2O_3 systems when
202 the mixture was sintered from 650 to 1050 ^oC for 3 h. After being sintered at 750 ^oC
203 for 3 h, the observable peaks show that the $CuFe_2O_4$ with tetragonal structure
204 (t-$CuFe_2O_4$) was first generated. Spinel-type ferrites usually display cubic symmetry
205 but some show tetragonal distortion in which one of the lattice edges differs in length
206 in relation to the other two.[35] Generally, in the normal AB_2O_4 spinel structure, B^{3+}
207 ions occupy some of the octahedral sites and A^{2+} ions locate on tetrahedral sites.[36] But
208 for an ideal inverse spinel, the Cu^{2+} ions occupy octahedral sites, whereas Fe^{3+} ions
209 are found on octahedral and tetrahedral sites with approximately equal occupancy.[35,37]
210 The t-$CuFe_2O_4$ is a stable low temperature phase, and its crystal lattice exhibits a
211 tetragonal distortion from the ideal inverse $CuFe_2O_4$ spinel.[35] From Figure 3, the
212 t-$CuFe_2O_4$ phase kept developing with elevated sintering temperatures, while peaks of
213 CuO and Fe_2O_3 diminished eventually. However, when the temperature reached 1000
214 ^oC, the $CuFe_2O_4$ phase mainly crystallized with cubic spinel structure with very strong
215 peak intensities, and the peaks of t-$CuFe_2O_4$ reduced dramatically. In cubic $CuFe_2O_4$
216 (c-$CuFe_2O_4$) crystal structure, a few of the Cu^{2+} ions occupy tetrahedral sites.[37] When
217 the sintering temperature kept increasing to 1050 ^oC, the orthorhombic compound
218 $CuFeO_2$ was detected. The formation of $CuFeO_2$ under air atmosphere was also
219 reported at a temperature range of 1000 to 1100 ^oC.[38,39].

220

The copper-hosting crystalline phases together with the other iron-hosting phases were all subjected to quantitative analysis via Rietveld refinement, and the weight fractions were shown in Figure 3a. Sintering the sample at 750 ^{o}C for 3 h generated around 75% of the t-$CuFe_2O_4$ phase, and the weight fractions of CuO and Fe_2O_3 reduced to values lower than 15%. With elevated temperatures, the weight percentage of t-$CuFe_2O_4$ phase increased to about 90% and kept stable around this value until the temperature reaching 950 ^{o}C. Further heating at 1000 ^{o}C cause the significant reduction of t-$CuFe_2O_4$ phase and substantial formation (about 70%) of the c-$CuFe_2O_4$ phase as observed in Figure 2. At 1050 ^{o}C, the c-$CuFe_2O_4$ developed with the weight percentage of higher than 80%, and about 20% of the $CuFeO_2$ was generated as another copper-hosting product phase.

Therefore, reactions derived from both XRD and quantitative results are listed below:

$$CuO + Fe_2O_3 \xrightarrow{\leq 950\ ^{o}C} CuFe_2O_4 \text{ (tetragonal)} \quad (1)$$

$$CuO + Fe_2O_3 \xrightarrow{1000\ ^{o}C} CuFe_2O_4 \text{ (cubic)} + CuFe_2O_4 \text{ (tetragonal)} \quad (2)$$

$$CuO + Fe_2O_3 \xrightarrow{1050\ ^{o}C} CuFe_2O_4 \text{ (cubic)} + CuFeO_2 \quad (3)$$

To indicate copper transformation efficiencies into different product phases, the transformation ratio (TR) is used. Taking M_n (n = 1, 2, 3,…) as copper-hosting product phases, the TR (n = 1, 2, 3,…) is calculated as follows:

243 TR (%)

244 $$= \frac{a_n \dfrac{\text{wt\% of } M_n}{\text{MW of } M_n}}{a_1 \dfrac{\text{wt\% of } M_1}{\text{MW of } M_1} + a_2 \dfrac{\text{wt\% of } M_2}{\text{MW of } M_2} + a_3 \dfrac{\text{wt\% of } M_3}{\text{MW of } M_3} + \cdots + a_n \dfrac{\text{wt\% of } M_n}{\text{MW of } M_n}} \quad (4)$$

245

246 where MW = molecular weight; a_n (n=1, 2, 3,…) is the number of the target copper
247 atom contained in the corresponding phase; and wt% is the weight fraction of its
248 corresponding phase obtained through Rietveld refinement..

249

250 Therefore, the TR index for copper transforming into t-$CuFe_2O_4$ (TR_t), c-$CuFe_2O_4$
251 (TR_c) and $CuFeO_2$ (TR_d) can be calculated according to Eq (4). And the total
252 transformation of copper (TR) into new crystal structures can be expressed as

253

254 $$TR\ (\%) = TR_t\ (\%) + TR_c\ (\%) + TR_d\ (\%) \quad (5)$$

255

256 The copper incorporation into t-$CuFe_2O_4$ reached around 70% at 750 °C and
257 increased to about 80% at the temperature range of 850-950 °C. The copper
258 transformation into c-$CuFe_2O_4$ increased significantly to around 60% after being
259 sintered at 1000 ^oC for 3 h. At the highest temperature (1050 ^oC) of this sintering
260 mechanism, about 73% of copper distributed in c-$CuFe_2O_4$ with 27% in $CuFeO_2$. The
261 total TR value kept stable around 80% at temperature ≤ 1000 ^oC, and reached 100% at
262 1050 ^oC, indicating the complete transformation of copper into product phases.

263

When the transformation behavior of copper in Fe_2O_3 and sewage sludge system is compared, it can be found that the tetragonal $CuFe_2O_4$ never appeared in sewage sludge system. Since a small amount of dopant ions can change structural properties of ferrites,[40] and the site preference of dopant ions might lead to transfer Fe^{3+} from A-sites to B-sites and cause a crystallographic transformation from tetragonal to cubic structure.[41] Therefore, the structure of the as formed $CuFe_2O_4$ in sewage sludge system will predominantly crystallize as cubic structure due to the existence and influence of Al,[42] Si,[43] or other minor compositions.

3.3. Leaching behavior of product phases

Because t-$CuFe_2O_4$ and c-$CuFe_2O_4$ are the potential and predominant copper-hosting phases in the sintered products, their capacity in metal stabilization must be taken into account and compared with the initial copper-containing phase (CuO). Thus, this study prepared single-phase samples to determine their intrinsic leachability and leaching behavior in a prolonged (22-d) leaching experiment. The as-received CuO powder was used as the single-phase sample after phase confirmation by XRD. The single-phase t-$CuFe_2O_4$ and c-$CuFe_2O_4$ sample were obtained by sintering the CuO + Fe_2O_3 mixture at 950 °C for 60 h and at 1000 °C for 72 h, respectively. The purpose of such prolonged sintering processes is to ensure the complete reaction at grain boundaries/surface. The XRD patterns of single-phase products are provided in Figure S5.

The pH value of the CuO leachate (Figure S6) underwent a significant increase in the first few days and then held steady at around pH 4.8. For c-$CuFe_2O_4$ and t-$CuFe_2O_4$ leachates, in contrast, were very close to the initial pH value of the leaching fluid throughout the leaching period. As an increase in leachate pH may be accompanied by the destruction of the sample crystal structure, the increase in the CuO leachate's pH may indicate that the CuO phase is more vulnerable to proton-mediated dissolution than the copper ferrite phases. Since the compositions of different metal-hosting phases will affect the contact between solid and solution, the total metal content should be normalized for comparison of the leachability. The normalized copper concentrations in both the CuO and copper ferrites leachates are presented in Figure 4a, which shows that the leached copper from the CuO sample is two orders greater than those from the $CuFe_2O_4$ samples. When the metal leachability of both ferrites is compared, the c-$CuFe_2O_4$ phase performed both higher copper and iron leaching than the lower temperature phase (t-$CuFe_2O_4$) as demonstrated in Figure 4a & b. At the end of the leaching period, a four-time higher copper concentration in c-$CuFe_2O_4$ leachate than that in t-$CuFe_2O_4$ leachate indicates the tetragonal $CuFe_2O_4$ phase as a more promising structure for copper stabilization. Moreover, the iron concentrations in t-$CuFe_2O_4$ leachate are lower than those in c-$CuFe_2O_4$ leachate, which confirms the higher resistance to acidic attack of the tetragonal structure.

With the proceeding of leaching process, the congruent dissolutions of these

crystalline phases in an acidic solution may be expressed as follows:

$$CuO_{(s)} + 2H^{+}_{(aq)} \rightarrow Cu^{2+}_{(aq)} + H_2O \quad (6)$$

$$CuFe_2O_{4(s)} + 8H^{+}_{(aq)} \rightarrow Cu^{2+}_{(aq)} + 2Fe^{3+}_{(aq)} + 4H_2O \quad (7)$$

The concentrations of both [Cu^{2+}] and [Fe^{3+}] may also be limited by the potential precipitation/dissolution of the $Cu(OH)_2$ and $Fe(OH)_3$ solid, respectively,[44,45] as listed in followings:

$$Cu(OH)_2 \leftrightarrow Cu^{2+} + 2OH^- \ (K_{spCu} = 10^{-19.3}) \quad (8)$$

$$Fe(OH)_3 \leftrightarrow Fe^{3+} + 3OH^- \ (K_{spFe} = 10^{-37.4}) \quad (9)$$

The pH value of the leachate at the end of the leaching process was measured as 4.9. According to Eq (8), the permitted [Cu^{2+}] value was calculated to be $10^{-1.1}$ M, which is higher than the measured total copper concentration of ~ 2090 mg L^{-1} (~ $10^{-1.5}$ M). Thus, copper ions might not be precipitated during the leaching process. Since the pH value of copper ferrite leachates kept stable at pH around 2.9, the system was maintained in a more acidic environment and the copper concentration was much lower than that of the CuO leachate. The copper concentrations in the leachates of c-$CuFe_2O_4$ and t-$CuFe_2O_4$ were all considerably under-saturated regarding to the

330 $Cu(OH)_{2(s)}$ phase. At pH 2.9, the permitted concentration of total Fe^{3+} ions is
331 calculated as $10^{-4.1}$ M (4.45 mg L^{-1}) according to Eq (9). From Figure 4b, the iron ion
332 concentrations were observed as 2.3 and 0.7 mg L^{-1} for c-$CuFe_2O_4$ and t-$CuFe_2O_4$,
333 respectively. The lower iron concentrations in both leachates than the permitted
334 maximum value shows that iron ions were also not subject to reprecipitation from the
335 leachates. Theoretically, if the c-$CuFe_2O_4$ and t-$CuFe_2O_4$ solid displayed a congruent
336 dissolution, the [Cu]/[Fe] molar ratios would be at 1:2 which is coincident with the
337 stoichiometry of Cu and Fe ions in their original phase. However, the observed
338 [Cu]/[Fe] molar ratios (> 1:2) in Figure 4c illustrate that both c-$CuFe_2O_4$ and
339 t-$CuFe_2O_4$ leachates are incongruent solutions, where the majority of the Fe-O bonds
340 still remained on copper ferrite surfaces.
341
342 Although c-$CuFe_2O_4$ and t-$CuFe_2O_4$ displayed incongruent leaching, the behavior in
343 both leachates is different from each other. Firstly, the [Cu]/[Fe] molar ratio decreased
344 from about 18.0 to around 8.0 and kept stable around 8.0 in t-$CuFe_2O_4$ leachates,
345 whilst the ratio in c-$CuFe_2O_4$ leachates kept stable from 4.3 to 5.0. Since both the
346 leaching of copper and iron increased with the prolong leaching time, the decrease of
347 [Cu]/[Fe] ratio might indicate the moderate leaching of copper from the tetragonal
348 structure. Secondly, although the [Cu]/[Fe] molar ratio kept decreasing within the first
349 10 days in t-$CuFe_2O_4$ leachates, the value of this ratio is still much higher than that in
350 c-$CuFe_2O_4$ leachates throughout the whole leaching process. The higher ratio means
351 that there might be more Fe-O bonds remained on the solid surface, which may inhibit

further leaching of copper from the product phase. Therefore, it might explain much lower copper leachability observed in t-$CuFe_2O_4$ leachates.

Even though with different treatment methods and leaching conditions, the effect of copper immobilization in this study was further compared with what have been reported in other studies. Kumpiene et al.[46] used coal fly ash and natural organic matter (peat) as the amendments to stabilize the metal contaminated soil, and reached a 98.2% decrease in the amount of leached copper. Solpuker et al.[47] investigated the potential of using pervious concrete to immobilize copper, and detected the degree of copper immobilization (the ratio of leached copper to initial copper amount) to be around 0.19. Furthermore, a recent study[48] reported that the combination treatment of calcined oyster shells (COS) and steel slag (SS) was sufficient enough to significantly decrease copper leachability (96% reduction). While in our study, a 99.7% and 99.4% decrease of the amount of leached copper was monitored for t-$CuFe_2O_4$ and c-$CuFe_2O_4$ phases compared to CuO, even with very fine milled powders and after a 22-d leaching period.

4. Conclusions

Copper ferrites were generated with two different crystal structures (cubic and tetragonal) when α-Fe_2O_3 was used as the ceramic precursor to incorporate copper, while the cubic $CuFe_2O_4$ was found as the only copper-containing product phase in

374 iron-rich municipal wastewater ash systems. The incorporation mechanisms of
375 hazardous copper were explicated with the combination of quantitative and qualitative
376 XRD technique. About 90% of the tetragonal $CuFe_2O_4$ phase was generated when
377 samples of $CuO+\alpha\text{-}Fe_2O_3$ were sintered at 850 ^oC for 3 h, while the weight percentage
378 of cubic $CuFe_2O_4$ phase increased to 70% with a significant decrease of tetragonal
379 $CuFe_2O_4$ when the samples were further heated at 1000 ^oC. Both copper ferrites
380 exhibited good performance in copper ion immobilization, and the low-temperature
381 tetragonal $CuFe_2O_4$ phase was further confirmed as a more promising structure for
382 copper stabilization when copper concentrations in both cubic and tetragonal $CuFe_2O_4$
383 leachates were compared. Although with different metal leachability, both cubic and
384 tetragonal $CuFe_2O_4$ displayed incongruent leaching behavior. In conclusion, through
385 reliably reusing iron-rich materials (the municipal wastewater sludge ash and iron
386 oxide), this study does not only show the potential to thermally stabilize the simulated
387 copper-polluted soils, but also realize the feasibility of achieving "waste-to-resource"
388 for a more sustainable environment.

389

390 **Acknowledgements**

391

392 This work was supported financially by Basic Research Funding from South
393 University of Science and Technology of China (FRG-SUSTC1501A-33), and the
394 General Research Fund Scheme of the Research Grants Council of Hong Kong (HKU
395 716310E). Dr. Chengshuai Liu also acknowledges the support from One Hundred

Talents Programme of the Chinese Academy of Sciences.

Supporting Information

One table and eight figures demonstrating the characterization of municipal wastewater sludge, powder XRD patterns of raw materials and pure phase products for leaching experiments, and two examples of Rietveld refinement results are available free of charge via the Internet at http://pubs.acs.org.

References

1. T. Kemper, S. Sommer, *Environ. Sci. Technol.* 2002, **36**, 2742−2747.
2. A. Navarro, E. Cardellach, M. Corbella, *J. Hazard. Mater.* 2011, **186**, 1576−1585.
3. E. Álvarez-Ayuso, A. García–Sánchez, *Sci. Total Environ.* **2003**, **305** (1–3), 1–12.
4. M. A. Yukselen, O. Gokyay, *Environ. Eng. Sci.* 2006, **23**, 125–132.
5. Y. H. Xu, D. Y. Zhao, *Environ. Sci. Technol.* 2005, **39**, 2369–2375.
6. Z. He, J. Fan, X. Yang, P. J. Stoffella, *Soil amendment to remediate copper contaminated soils.* 19th World Congress of Soil Science, Soil Solutions for a Changing World. Brisbane: Australia, 2010.
7. C. N.Mulligan, R. N. Yong, B. F. Gibbs, *Eng. Geol.* 2001, **60**, 193–207.
8. J. Kumpiene, A. Lagerkvist, C. Maurice, *Waste Manag.* 2008, **28**, 215–225.
9. P. Janoš, J. Vávrová, L. Herzogová, V. Pilařová, *Geoderma* 2010, **159**, 335–341.
10. H. A. van der Sloot, L. Heasman, P. H. Quevauviller, *Harmonization of Leaching/Extraction Tests*. Elsevier: Amsterdam, the Netherlands, 1997.
11. K. Shih, T. White, J. O. Leckie, *Environ. Sci. Technol.* 2006, **40**, 5520–5526.
12. K. Shih, T. White, J. O. Leckie, *Environ. Sci. Technol.* 2006, **40**, 5077–5083.
13. Y. Tang, K. Shih, K. Chan, *Chemosphere* 2010, **80**, 375–380.
14. Y. Tang, S. S.-Y. Chui, K. Shih, L. Zhang, *Environ. Sci. Technol.* 2011, **45**, 3598–3604.
15. C. R. Cheeseman, G. S. Virdi, *Resour. Conserv. Recy.* 2005, **45**, 18–30.
16. J. Werther, T. Ogada, *Prog. Energy Combust. Sci.* 1999, **25**, 55–116.
17. A. Fullana, J. A. Conesa, R. Font, S. Sidhu, *Environ. Sci. Technol.* 2004, **38**, 2953–2958.
18. D. Fytili, A. Zabaniotou, *Renew. Sust. Energ. Rev.* 2008, **12**, 116–140.
19. R. D. Davis, *Water Environ. J.* 1996, **10** (1), 65–69.
20. Public Works Subcommittee of Finance Committee. *Environmental Protection–Sewerage and Sewage Treatment 233DS–Sludge Treatment Facilities*. Hong Kong Environmental Production Department (HKEPD): Hong Kong, 2009.
21. L. Spinosa, A. Ayol, J. C. Baudez, R. Canziani, P. Jenicek, A. Leonard, W. Rulkens, G. Xu, L. van Dijk, *IWA Publishing* 2011, **3**, 702–717.
22. T. Murakami, Y. Suzuki, H. Nagasawa, T. Yamamoto, T. Koseki, H. Hirose, S. Okamoto, *Fuel Process. Technol.* 2009, **90**, 778–783.
23. O. ;Malerius, J. Werther, *Chem. Eng. J.* 2003, **96**, 197–205.

24. R. Kikuchi, *J. Air Waste Manage. Assoc.* 1998, **48**, 1112–1115.
25. W. Rulkens, *Energ. Fuel.* 2008, **22**, 9–15.
26. G. R. Xu, Z. C. Yan, Y. C. Wang, N. Wang, *J. Hazard. Mater.* 2009, **161** (2–3), 663–669.
27. M. Cyr, M. Coutand, P. Clastres, *Cem. Concr. Res.* 2009, **37** (8), 1278–1289.
28. G. Merrington, I. Oliver, R. J. Smernik, M. J. McLaughlin, *Adv. Environ. Res.* 2003, **8**, 21–36.
29. Drainage Services Department; Environmental Protection Department. Treatment and disposal of sewage sludge (Chapter 8) in *Audit Commission.* Hong Kong Environmental Production Department (HKEPD): Hong Kong, 2007; http://www.environmental-auditing.org/Portals/0/AuditFiles/Hongkong_full_eng_07_sewage_sludge.pdf
30. J. Bratby, *IWA Publishing* 2006, **21**, 25–27.
31. M. Hartman, M. Pohořelý, O. Trnka, *Chem. Pap.* 2007, **61** (3), 181–185.
32. R. A. Young, *The Rietveld Method*, *(2nd ed.).* Oxford University Press: New York, American, 1993.
33. R. Brett, *Geochim. Cosmochim. Acta*, 1992, **56**, 3603–3606.
34. Y. J. Park, S. O. Moon, J. Heo, *Ceram. Int.* 2003, **29**, 223–227.
35. M. Ristić, B. Hannoyer, S. Popović, S. Musić, N. Bajraktaraj, *Mater. Sci. Eng.* 2000, **77**, 73–82.
36. C. B. Carter, M. G. Norton, *Ceramic Materials: Science and Engineering*. New York, Springer: London, 2007.
37. D. Thapa, N. Kulkarni, S. N. Mishra, P. L. Paulose, P. Ayyub, *J. Phys. D. Appl. Phys.* 2010, **43**, 195004 (1–5).
38. M. A. Zinovik, *Russ. J. Inorg. Chem. (Engl. Transl.)* 1988, **33**(10), 1543–1545.
39. Materials Science International Team (MSIT). *Selected Systems from Co–Fe–Si to Cu–Fe–Pt (Landolt–Börnstein: Numerical Data and Functional Relationships in Science and Technology – New Series / Physical Chemistry)*, Springer: London, 2008.
40. K. S. Lohar, S. M. Patange, S. E. Shirsath, V. S. Surywanshi, S. S. Gaikwad, S. S. Jadhav, N. Kulkarni, *IJAET* 2012, **3**(1), 354–361.
41. S. S. Ata-Allah, F. M. Sayed–Ahmed, M. Kaiser, A. M. Hashhash, *J. Mater. Sci.* 2005, **40**, 2923–2930.
42. N. M. Deraz, *J. Anal. Appl. Pyrolysis* 2008, **82**, 212–222.
43. H. M. Zaki, S. F. Mansour, *J. Phys. Chem. Solids* 2006, **67**, 1643–1648.

44. W. Stumm, J. J. Morgan, *Aquatic Chemistry Chemical Equilibria and Rates in Natural Waters (3rd ed.).* Wiley: New York, 1996.

45. S. S. Zumdahl, *Chemical Principles (Enhanced ed.)*. Brooks Cole: Belmont, CA, 2010.

46. J. Kumpiene, A. Lagerkvist, C. Maurice, *Environ. Pollut.* 2007, **145**, 365-373.

47. U. Solpuker, J. Sheets, Y. Kim, F. W. Schwartz, *J. Contam. Hydrol.* 2014, **161**, 35-48.

48. D. H. Moon, M. Wazne, K. H. Cheong, Y.-Y. Chang, K. Baek, Y. S. Ok, J.-H. Park, *Environ. Sci. Pollut. Res.* 2015, **22**, 11162–11169.

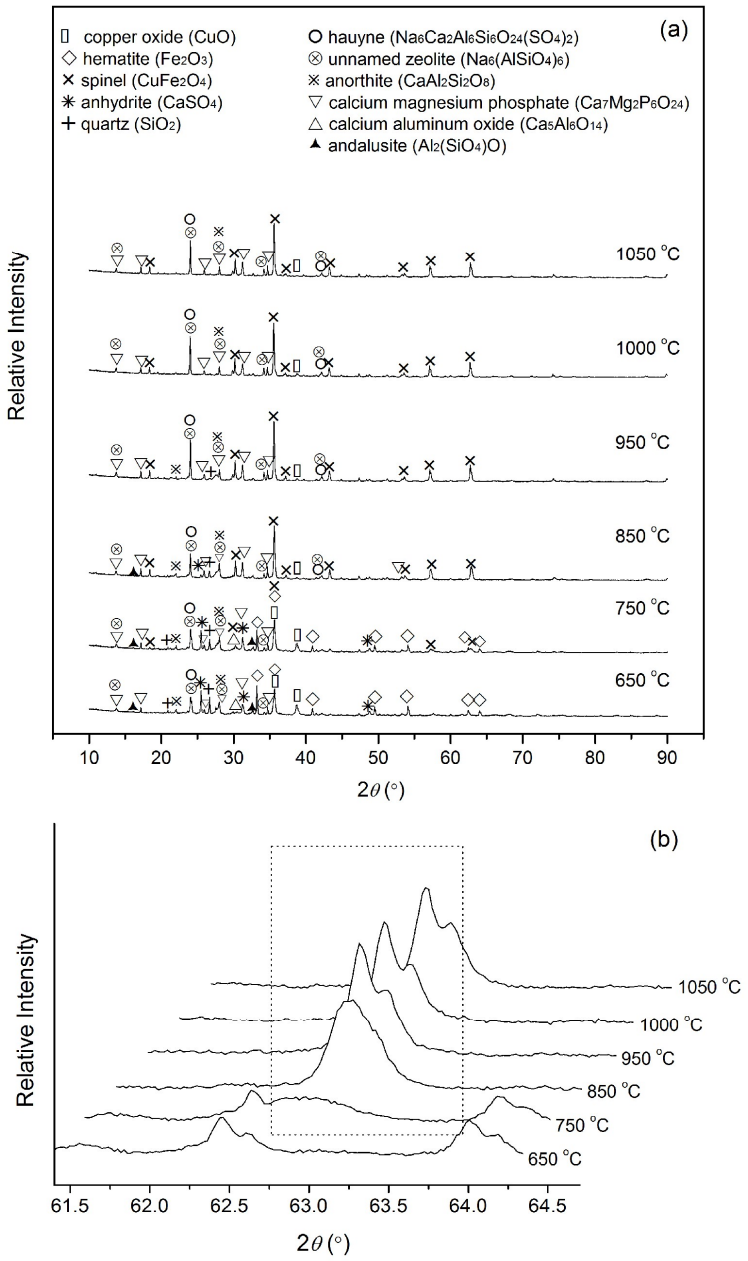

Figure 1. (a) XRD patterns of the sludge ash + CuO system, and (b) the comparison of XRD peak intensities (between 2θ = 61.5 and 64.5°) for sludge ash + CuO samples sintered at 650-1050 °C for 3 h. The crystalline phases are identified as: CuO (PDF#80-1268), Fe_2O_3 (PDF#85-0599), $CuFe_2O_4$ (PDF#77-0010), anhydrite ($CaSO_4$, PDF#37-1496), quartz (PDF#79-1910), hauyne ($Na_6Ca_2Al_6Si_6O_{24}(SO_4)_2$, PDF#73-1920), unnamed zeolite ($Na_6(AlSiO_4)_6$, PDF#42-0217), anorthite ($Ca(Al_2Si_2O_8)$, PDF#89-1473), calcium magnesium phosphate ($Ca_7Mg_2P_6O_{24}$, PDF#20-0348), calcium aluminum oxide ($Ca_5Al_6O_{14}$, PDF#11-0357), andalusite ($Al_2(SiO_4)O$, PDF#39-0376).

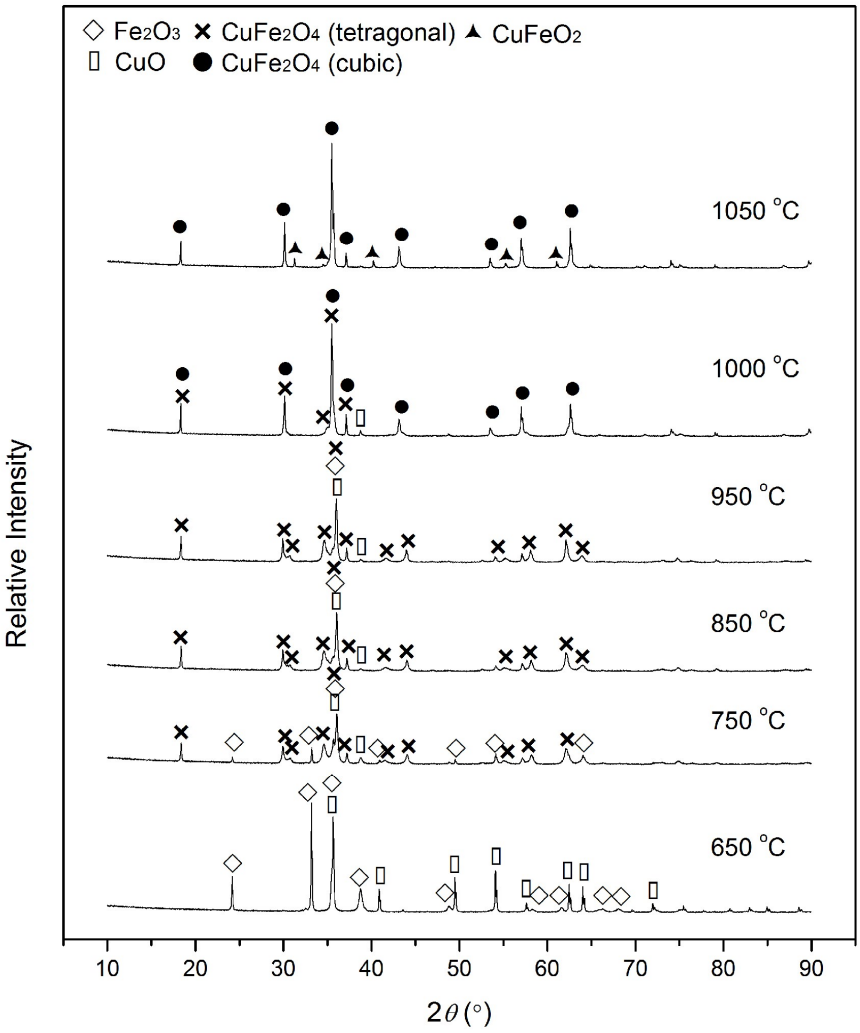

Figure 2. XRD patterns of 650-1050 °C and 3 h sintered Fe_2O_3 + CuO samples. The standard patterns include CuO (PDF#80-1268), tetragonal $CuFe_2O_4$ (PDF#34-0425), cubic $CuFe_2O_4$ (PDF#77-0010), $CuFeO_2$ (PDF#75-2146), and hematite (α-Fe_2O_3, PDF#85-2599).

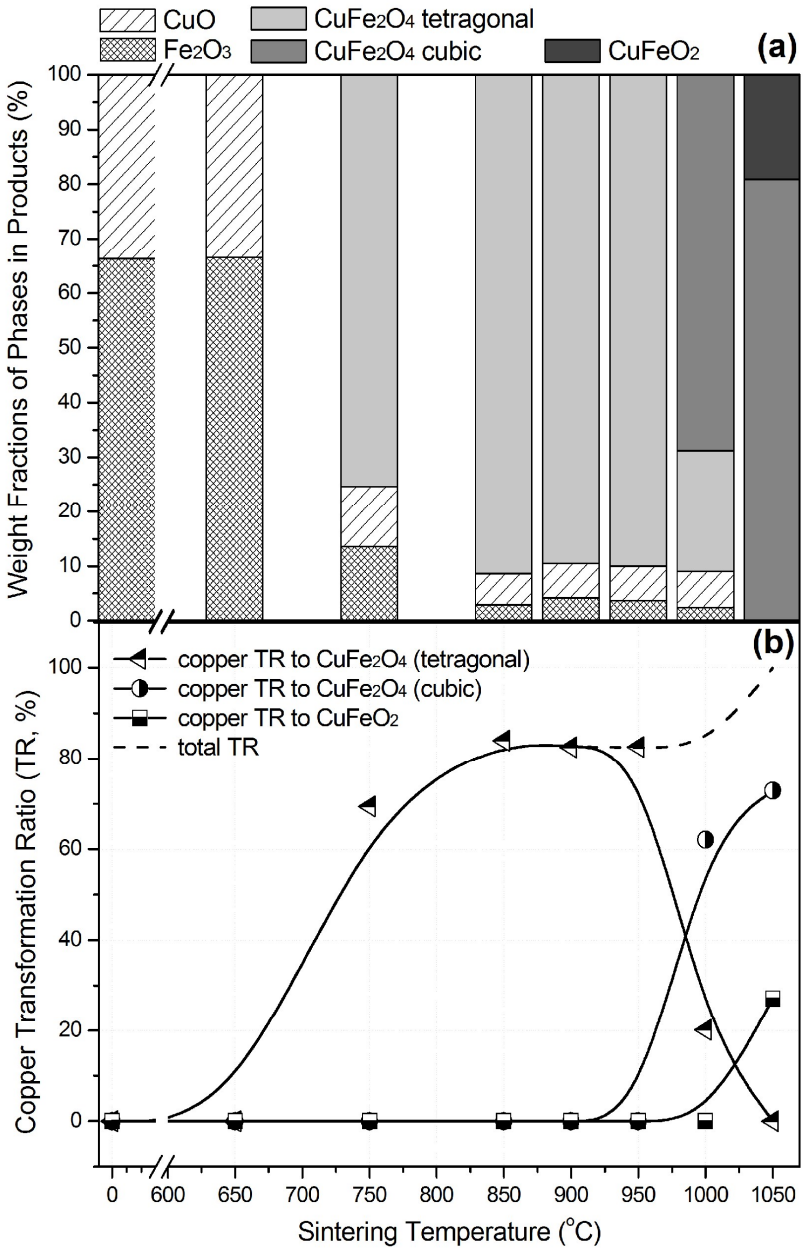

503
504
505 Figure 3. (a) Variations of weight fractions of Cu- and Fe-containing crystalline
506 phases obtained from the CuO sintering reactions with Fe_2O_3 precursor, and (b) the
507 transformation ratios (TR_t, TR_c. TR_d, and total TR, %) of Cu into the product phases.
508
509

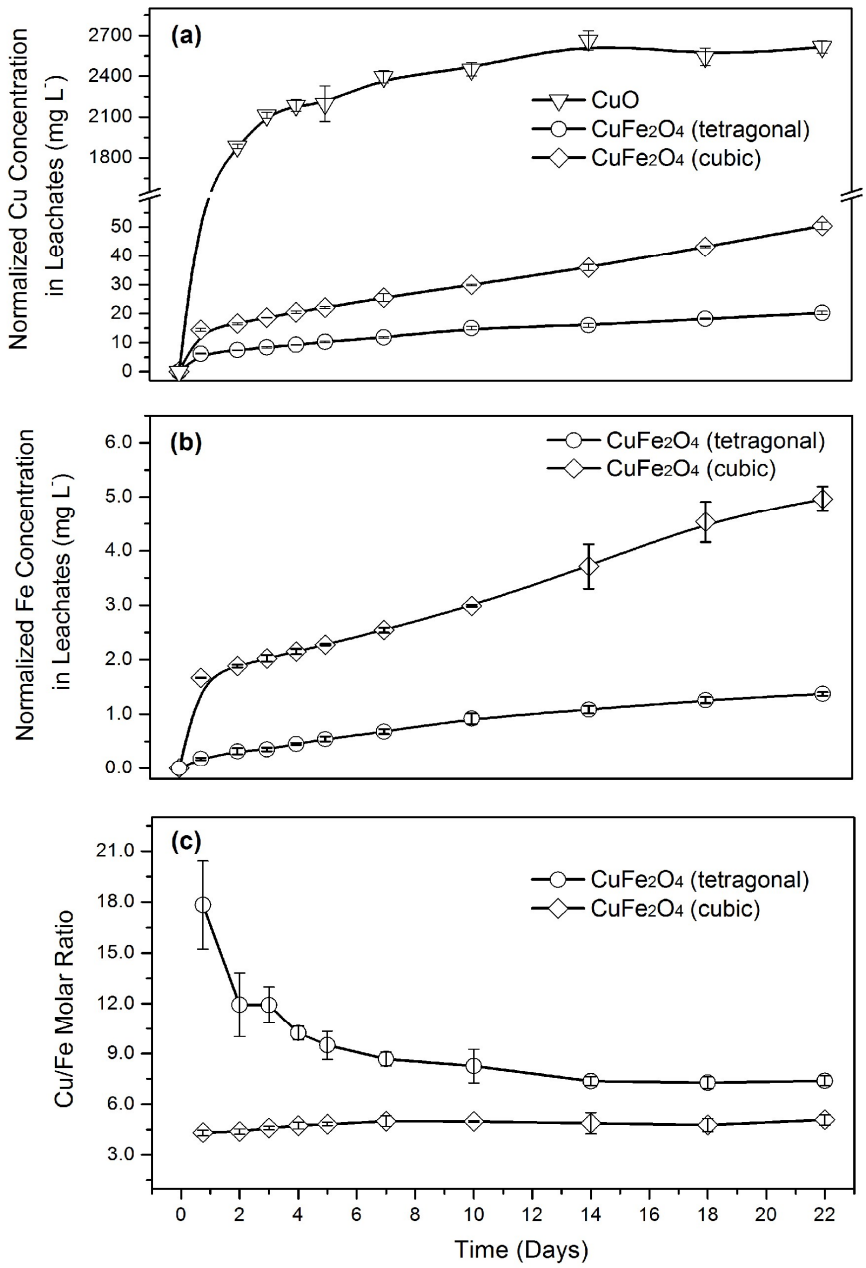

Figure 4. (a) Normalized copper concentrations of the CuO, tetragonal $CuFe_2O_4$, and cubic $CuFe_2O_4$ leachates, (b) normalized iron concentrations and (c) [Cu]/[Fe] molar ratios of tetragonal $CuFe_2O_4$ and cubic $CuFe_2O_4$ leachates. The leaching solution was TCLP extraction fluid no. 2 (acetic acid solution) with a pH of 2.9. Each leaching vial was filled with 10 ml of extraction fluid and 0.5 g of powder samples, and then rotated end-over-end between 0.75 and 22 d.

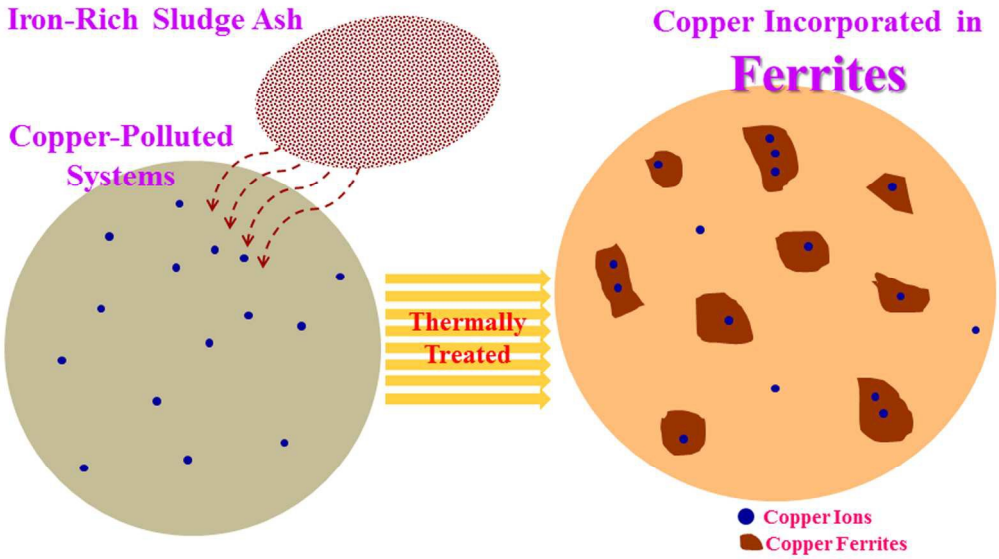

150x84mm (300 x 300 DPI)